

Deformation of Wilcox shale: Undrained strengths and effects of strain rate

Ohmyoung Kwon & Andreas K. Kronenberg

Department of Geology and Geophysics, Center for Tectonophysics, Texas A&M University,
College Station, Tex., USA

ABSTRACT: Mechanical and fluid transport properties of brine-saturated illite shale from the Wilcox Formation have been investigated to examine the effects of strain rate on fracture strength and to determine the conditions over which rates of deformation and internal fluid flow compete. Permeability (k) measurements predict time scales for fluid pressure equilibration that are long relative to those of deformation experiments; values of k are small even at relatively low effective pressures P_e (assumed $\cong P_c - P_f$) and they drop below 10^{-20} m^2 at pressures of $\geq 5 \text{ MPa}$. Failure strengths ($\sigma_1 - \sigma_3$) of Wilcox shale specimens saturated (as nearly as can be achieved) with brine and shortened at strain rates of $2.8 \times 10^{-7} \leq \dot{\epsilon} \leq 8.2 \times 10^{-3} \text{ s}^{-1}$ fit an exponential law $\dot{\epsilon} = A \exp\{\alpha(\sigma_1 - \sigma_3)\}$ of the same form as determined for Wilcox shale specimens deformed at much higher pressures in the absence of pore fluids. The positive slope and comparable value of α ($= 0.29 \text{ MPa}^{-1}$) to that determined for specimens without pore fluids ($\alpha = 0.3 \text{ MPa}^{-1}$) suggest that Wilcox shale exhibits undrained behavior at strain rates $> 10^{-7} \text{ s}^{-1}$ and that strain rate effects associated with pore pressure perturbations and pore fluid transport occur at much lower strain rates.

1 INTRODUCTION

Clay-rich shales deform readily in a variety of geologic settings in response to tectonic and depositional loads that are relatively small, yet laboratory experiments performed on clay-bearing shales in the absence of pore fluids reveal significant strengths that are comparable to those measured for higher grade rocks such as slates and mica-bearing schists (Shea and Kronenberg 1992, Ibanez and Kronenberg 1993). Low strengths are required of shales that make up basal detachments of thin-skinned thrust sheets (Chapple 1978) as well as shale units that develop into diapir structures (Bishop 1977). Fluid-saturated shales have low strengths primarily due to elevated pore pressures and correspondingly low effective pressures that may be maintained over extended periods of time. Experimental studies on shales indicate that shear strengths of fluid-saturated shales are lower than those of dry shales and undrained compressive strengths are lower than drained strengths (Mesri and Gibala 1972, Van Eeckhout 1976, Bauer 1979, Cook 1989, Steiger and Leung 1990, Nuesch 1991).

Shales may exhibit undrained mechanical response over a wide range of conditions due to permeabilities that are very low. Changes in stress state during deformation experiments can give rise to pore pressure perturbations within specimen interiors that are not reflected in fluid pressures measured at specimen extremities and failure will be governed by deformation in regions of elevated pore pressure. As strain rates are reduced and times available for fluid transport are increased, rates of deformation and fluid flow may compete giving rise to strengths that depend upon strain rate (Swan et al. 1989), and at very low strain rates, shales may exhibit drained response.

A variety of deformation mechanisms may exhibit critical thresholds for their activation that depend on the rate of deformation and previous experiments performed on Wilcox shale specimens at high pressures in the absence of pore fluids reveal an intrinsic effect of strain rate on inelastic strength (Ibanez and Kronenberg 1993). Compressive differential stresses ($\sigma_1 - \sigma_3$) measured at confining pressures (P_c) of 250 MPa both at the onset of yielding and at failure increase with increasing strain rate ($\dot{\epsilon}$) and fit an exponential law $\dot{\epsilon} = A(T) \exp\{\alpha(\sigma_1 - \sigma_3)\}$ where $A(T)$ depends on temperature and α is a material parameter.

Similarly, increases in failure strengths of fluid-saturated Kimmeridge Bay shale specimens were observed with increasing strain rate (Swan et al. 1989) at strain rates ($\dot{\epsilon} > 10^{-4} \text{ s}^{-1}$) sufficiently rapid to preclude loss of any pore fluids during deformation. However, Swan et al. (1989) also reported a transition in mechanical response at lower strain rates with an inverse relationship between strength and strain rate that was inferred to reflect internal fluid flow and the decay of local pore pressure perturbations at longer time scales. Characteristic times over which fluid pressures equilibrate may differ amongst different shales depending upon their permeabilities and the length scales over which fluid flow must occur. The strain rates at which other shales exhibit the transition in mechanical behavior reported for Kimmeridge Bay shale therefore depend upon the complex distributions of interconnected pores that govern permeability and interactions with microcracks that are generated during deformation.

In this paper, we present experimental determinations of fluid flow and fracture strength over a wide range in strain rate for brine-saturated Wilcox shale in order to determine the conditions required for drained, undrained, and transitional mechanical responses. The results suggest that strain rate effects associated with transient pore pressure perturbations occur at very low strain rates ($< 10^{-7} \text{ s}^{-1}$), well below those investigated in this study. The observed dependence of failure strength on strain rate appears to reflect the undrained mechanical behavior of Wilcox shale. Remarkably, the undrained strength-strain rate relationship parallels the intrinsic material response of Wilcox shale observed at high confining pressures in the absence of pore fluids.

2 EXPERIMENTAL METHODS

2.1 Starting material

Shale specimens were prepared from cores of the Wilcox Formation recovered from depths of approximately 3,960 m from West Baton Rouge Parish, Louisiana. Wilcox shale is rich in illite and chlorite, and clay minerals make up 55% of this shale. Porosities range from 2.5% in the clay-rich sections to 15% in the silty and quartz-rich sections; however, most of the specimens tested in this study are rich in clay and low in porosity. X-ray pole figure goniometry and SEM observations indicate that clay minerals are aligned parallel to the bedding plane with an illite preferred orientation that is comparable to those of many other deeply-buried shales but weak relative to layer silicate preferred orientations of slates and schists. This material has been characterized by Ibanez and Kronenberg (1993) and its mechanical properties in the absence of pore fluids were determined at strain rates of 2.3×10^{-7} to $1.0 \times 10^{-3} \text{ s}^{-1}$ at high confining pressures ($P_c \geq 200 \text{ MPa}$).

2.2 Experimental techniques

Right cylindrical specimens of Wilcox shale were cored parallel to bedding (12.5 mm diameter) and ends ground parallel (specimen length = 25.4 mm). Measurements of permeability and compressive strength in the presence of brine were made at pressure using the same apparatus (Fig. 1). Measurements of permeability along the axes of specimens (parallel to bedding) were made using a simple transient pulse technique (Brace et al. 1968, Sutherland and Cave 1980). Fluid pressures were measured at both

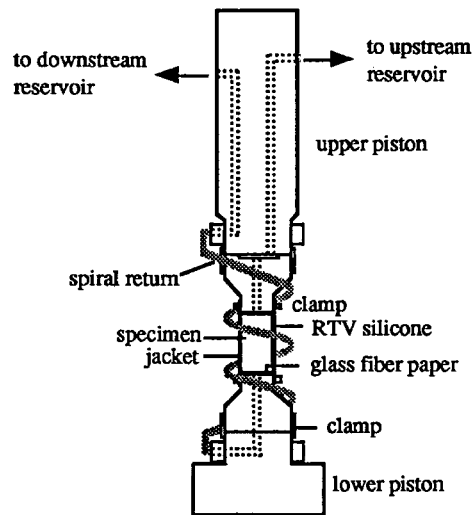


Figure 1. Schematic configuration of specimen assembly used in triaxial deformation apparatus, both for permeability measurements and for deformation experiments.

ends of each specimen by means of two access ports within the top piston, a spiral return line (Fig. 1), and high sensitivity Dynisco PT130 transducers. A small stepwise change in fluid pressure was applied to one end of the specimen and decay in the difference in fluid pressures across the specimen was measured as a function of time. Failure strengths were measured for specimens that were confined laterally and loaded axially (parallel to bedding) with known fluid pressures at specimen ends.

Permeabilities were determined using 1M NaCl solutions that filled the volume of the apparatus fluid pressure system and were introduced into specimen pores by multiple vacuum impregnation procedures performed over several days. A thin coat of RTV silicone was applied on the lateral surfaces of specimens before inserting them into heat shrinkable polyolefin jackets in order to prevent fluid flow between the jacket and specimen. Layers of glass fiber paper were placed on both ends of the specimen to ensure uniform access of pore fluid to the specimen ends. Tests performed on an aluminum specimen using these methods indicate that flow between the lateral specimen surface and jacket does not occur for confining pressures (P_c) that are greater than fluid pressure (P_f) by ≥ 0.5 MPa. Effective volumes of upstream (15 ml) and downstream (24 ml) reservoirs of the fluid pressure system were determined after purging the system of air and these values were used for permeability determinations.

After the specimen assembly was placed within the pressure vessel, the specimen and that portion of the pore pressure system that required disassembly between experiments were placed under a vacuum for 1 hour to remove air trapped in the system. The system was then filled with NaCl solution and bled repeatedly to ensure complete filling by the fluid. After filling the system with NaCl solution, confining pressure (P_c) and fluid pressure (P_f) were increased stepwise over an extended period of time to the desired experimental conditions, taking care that the difference between confining and fluid pressures did not exceed the pressure difference ($P_c - P_f$) at which permeability was to be measured. Several (2 to 4) days were generally required for fluid pressures to reach equilibrium, depending on the values of P_c and P_f desired. Once fluid pressures achieved equilibrium, the upstream reservoir was isolated from the downstream reservoir and the pressure in the upstream reservoir was increased stepwise at time $t = 0$ by a small amount (ΔP_i). The decay of the fluid pressure difference $\Delta P (= P_{up} - P_{dn}$ where P_{up} and P_{dn} are fluid pressures in the upstream and downstream reservoirs,

respectively) across the specimen was then monitored as a function of time. Measurements of ΔP exhibited decay consistent with the expression (Sutherland and Cave 1980):

$$(1) \quad (P_{up} - P_{dn}) = \Delta P_i e^{-\alpha t}$$

within experimental error, where ΔP_i is the initial pressure difference at time $t = 0$ and

$$(2) \quad \alpha = (kA/\mu\beta L)(1/V_{up} + 1/V_{dn})$$

where k is permeability, A and L are, respectively, the cross-sectional area and length of the specimen, μ is the viscosity and β is the compressibility of the fluid, and V_{up} and V_{dn} are upstream and downstream reservoir volumes, respectively. Values of viscosity (9.9×10^{-10} MPa-s) and compressibility (4.56×10^{-4} MPa $^{-1}$) for the brine were assumed to be similar to those of water, taken from the ASME steam tables (Meyer et al. 1979). The fluid pressures (P_f) reported in Table 1 are those at equilibrium with the specimen before applying the step in the upstream reservoir pressure.

Triaxial compression experiments were performed on shale specimens impregnated with 1M NaCl solution, using the same assembly (Fig. 1) as used for permeability measurements. Experiments were conducted over a range of initial effective pressures, P_e ($\cong P_c - P_f = 3$ to 10 MPa) at a strain rate of 1.5×10^{-5} s $^{-1}$ and over a range of strain rates (from 2.8×10^{-7} to 8.2×10^{-3} s $^{-1}$) at an effective pressure of 5.5 MPa (with $P_c = 10, 13,$ and 21.5 MPa, and externally determined $P_f = 4.5, 7.5,$ and 16 MPa, respectively). Because pressures were allowed to equilibrate over extended times prior to the deformation experiments, external measures of fluid pressures may provide true values of pore pressures within specimens at the onset of deformation. However, we cannot be certain that internal pore pressures were equivalent to externally measured fluid pressures during the deformation experiments once differential stresses were applied. Specimen dimensions and procedures to fill the pore pressure system were the same as those used for permeability measurements. However, the upstream and downstream fluid reservoirs were not isolated during deformation experiments. Fluid pressure was applied at both specimen ends and fluids were allowed to drain at both ends of each specimen. Fluid pressures were not adjusted during deformation experiments; instead, external fluid pressures were monitored during deformation. All permeability measurements and deformation experiments were performed at room temperature.

3 RESULTS AND DISCUSSION

Representative results used to determine permeabilities are illustrated in Figure 2A and permeability measurements are summarized in Table 1 and Figure 2B. Results of deformation experiments are shown in Figures 3 and 4 and listed in Tables 2 and 3.

3.1 Permeability measurements

Wilcox shale exhibits permeabilities (k) to brine that are very small and long times were required for each measurement of k . The decay in fluid pressure P_{up} and growth of P_{dn} (Fig. 2A) were monitored continuously for each determination of k until the difference between the two dropped below 50% of the initial pressure difference ΔP_i imposed. Daily fluctuations in fluid pressures due to fluctuations in room temperature ($\pm 2^\circ$) were minimized by insulation that was wrapped around the fluid reservoirs and plumbing. However, the difference between the two pressures ($P_{up} - P_{dn}$) was much less sensitive to temperature fluctuations and values of k were determined from the decline in $\log(P_{up} - P_{dn})$ with time (Fig. 2A) using eqns. (1) and (2).

Permeabilities of rocks are generally observed to vary with effective pressure and

Table 1. Permeability results for Wilcox shale.

Specimen Number	P_c (MPa)	P_f (MPa)	$P_c - P_f$ (MPa)	ΔP_i (MPa)	Permeability ($\times 10^{-21} \text{ m}^2$)
WFS 2-7A	13	10	3	2	141 (± 2.5)
WFS 6-1A	15	12	3	1.5	16.8 (± 0.2)
WFS 7-6	16.5	13.5	3	1.5	26.9 (± 0.4)
WFS 6-1B	16	12	4	1.5	12.9 (± 0.1)
WFS 6-1C	17	12	5	1.5	9.0 (± 0.3)
WFS 5-9	13	7.5	5.5	1.5	8.9 (± 0.2)
WFS 7-2	25.5	20	5.5	2	4.4 (± 0.3)
WFS 2-7B	18	10	8	2	2.4 (± 0.1)
WFS 6-1D	20	12	8	1.5	6.6 (± 0.1)

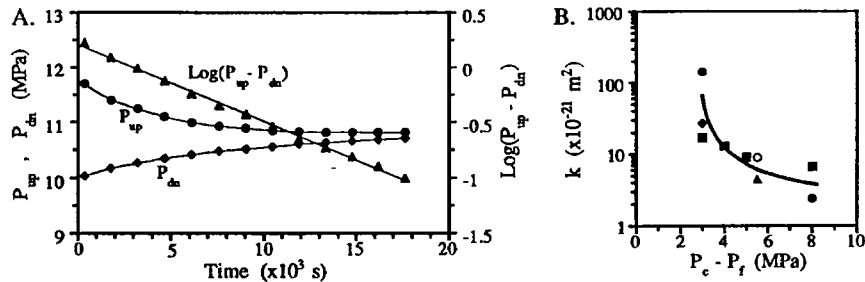


Figure 2. Permeability results. (A) Pressure changes in upstream (P_{up} , shown as circles), and downstream (P_{dn} , as diamonds) reservoirs with time, as well as $\log(P_{up} - P_{dn})$ with time (shown as triangles) for Wilcox shale (WFS2-7A) at $P_c - P_f = 3$ MPa where P_c and P_f are confining and fluid pressures, respectively, before imposing ΔP_i . A permeability $k = 1.41 \times 10^{-19} \text{ m}^2$ is given by the slope in $\log(P_{up} - P_{dn})$ vs. t and application of eqns. (1) and (2). (B) Permeability (k) as a function of $(P_c - P_f)$. Results shown for experiments performed at fluid pressures of 7.5 (open circle), 10 (filled circle), 12 (square), 13.5 (diamond), and 20 MPa (triangle).

measurements of k for transport in Wilcox shale parallel to bedding (Fig. 2B) show a strong dependence on $(P_c - P_f)$, the difference between confining pressure and fluid pressure. The pressure difference $(P_c - P_f)$ may not be a true measure of effective pressure for transport properties and values of k measured at the same $(P_c - P_f)$ but different P_c show some scatter. Further experiments are needed to explore the dependence of k on P_c and P_f ; nevertheless, a general trend is clearly defined and permeabilities drop below 10^{-20} m^2 at $(P_c - P_f) \geq 5$ MPa (Fig 2B).

Depending upon the scale at which fluid flow occurs, characteristic times for pore pressure equilibration can be determined from values of k (Rice and Cleary 1976, Roeloffs 1988) and used to evaluate whether perturbations in pore pressure associated with deformation are likely to be generated. For pore pressure equilibrium at the specimen scale, time intervals greater than 2×10^5 s (56 hours) are required (using $k = 8.9 \times 10^{-21} \text{ m}^2$ at $P_c - P_f = 5.5$ MPa, specimen WFS5-9, assuming that flow is one-dimensional, eqn. (23) of Roeloffs, 1988, and that fluid pressure perturbations decay by $\geq 90\%$). Fluid flow at the specimen scale is negligible at times less than 1.5×10^3 s (25 minutes) and external measures of fluid pressure over time intervals less than this cannot be expected to track pore pressures within the specimen interior. Alternatively, fluid flow may be important at much finer scales associated with equilibration of fluid pressures between nearby pores and dilatant microcracks. For fluid flow over length scales of ~ 0.5 mm, near-equilibrium can be achieved in times of > 370 s (6 minutes) while fluid pressures may be spatially very heterogeneous at times < 3 s.

Table 2. Mechanical results for Wilcox shale at $\dot{\epsilon} = 1.5 \times 10^{-5} \text{ s}^{-1}$.

Specimen Number	P_c (MPa)	P_f (MPa)	$P_c - P_f$ (MPa)	$\sigma_1 - \sigma_3$ (MPa)
WFS 2-4	10	7	3	8.0
WFS 7-6	16.5	13.5	3	32.0
WFS 7-5	18	15	3	19.3
WFS 7-1	21.5	16	5.5	37.0
WFS 2-7	20	10	10	47.0

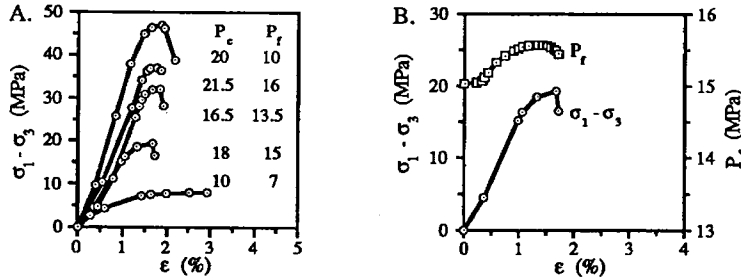


Figure 3. Mechanical results. (A) Differential stress-strain ($\sigma_1 - \sigma_3$ vs. ϵ) curves for Wilcox shale specimens deformed at a strain rate of $1.5 \times 10^{-5} \text{ s}^{-1}$ (values of P_c and P_f given in MPa). (B) Differential stresses ($\sigma_1 - \sigma_3$) and fluid pressures (P_f) measured at the ends of the specimen as functions of shortening strain (ϵ) for Wilcox shale (WFS7-5) at $P_c = 18$ and initial $P_f = 15$ MPa.

3.2 Triaxial deformation

Triaxial deformation experiments conducted at a strain rate of $1.5 \times 10^{-5} \text{ s}^{-1}$ over a range of confining pressures and initial fluid pressures reveal a general trend of increasing strength with increasing effective pressure (Fig. 3A) associated with the development of sharply defined shear fractures, similar to results obtained at low confining pressures for Wilcox shale without pore fluids (Ibanez and Kronenberg 1993). Confining and fluid pressures were applied over times sufficiently long prior to the deformation experiments to achieve equilibrium pore pressures at their outset. However, time scales for fluid flow at the specimen scale predicted by permeability measurements exceed the time intervals over which the stress state changes at $\dot{\epsilon} = 10^{-5} \text{ s}^{-1}$, and the results for three specimens deformed at initial effective pressures of 3 MPa (Fig. 3A) but at different confining pressures show wide variations in strength. Fluid pressures monitored during deformation increased as differential stresses increased and began to decrease near failure (Fig. 3B) indicating that some fraction of the pore fluid was initially expelled and later drawn into specimens during deformation. However, the variations in failure strength at given values of initial effective pressure ($P_c - P_f$) suggest that specimens deformed at $\dot{\epsilon} = 10^{-5} \text{ s}^{-1}$ exhibit essentially undrained behavior.

Given that small fluctuations in fluid pressures at specimen extremities were detected at $\dot{\epsilon} = 10^{-5} \text{ s}^{-1}$, deformation experiments on Wilcox shale were conducted at strain rates from 2.8×10^{-7} to $8.2 \times 10^{-3} \text{ s}^{-1}$ to test for effects of transient pore pressures at the same confining and fluid pressures ($P_c = 13$ MPa and $P_f = 7.5$ MPa, respectively) as were applied during permeability measurements. The mechanical results of two additional specimens (WFS7-1 and WFS5-7) deformed at an initial effective pressure (P_c) of 5.5 MPa were also used to examine effects of strain rate, although the confining pressures applied during these experiments differed from those of the other experiments ($P_c = 21.5$ MPa and $P_c = 10$ MPa, respectively). Combined, these experiments reveal an increase in failure strength with increasing strain rate (Fig. 4A), a result that differs from anticipated strain rate effects associated with pore fluid transport and is more readily explained if specimens remain undrained during deformation over the entire

Table 3. Mechanical results for Wilcox shale at $P_c - P_f = 5.5$ MPa.

Specimen Number	P_c (MPa)	P_f (MPa)	$P_c - P_f$ (MPa)	$\dot{\epsilon}$ (s^{-1})	$\sigma_1 - \sigma_3$ (MPa)
WFS 7-8	13	7.5	5.5	2.8×10^{-7}	20.5
WFS 5-7	10	4.5	5.5	3.0×10^{-7}	31.1
WFS 5-1	13	7.5	5.5	8.1×10^{-7}	29.5
WFS 7-1	21.5	16	5.5	1.5×10^{-5}	37.0
WFS 5-2	13	7.5	5.5	8.2×10^{-5}	40.2
WFS 5-4	13	7.5	5.5	2.3×10^{-3}	57.9
WFS 5-8	13	7.5	5.5	8.2×10^{-3}	60.8

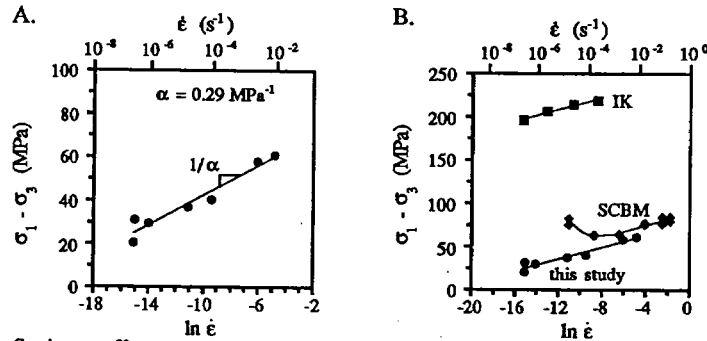


Figure 4. Strain rate effects on strength of shale. (A) Differential stress ($\sigma_1 - \sigma_3$) measured at failure vs. $\ln \dot{\epsilon}$ for experiments performed on Wilcox shale specimens at an initial effective pressure (given by externally measured P_f) of 5.5 MPa. Assuming eqn. (3), the slope is given by $1/\alpha$ with $\alpha = 0.29$ MPa^{-1} . (B) Comparison of the results of this study with those for dry Wilcox shale at high confining pressures ($\alpha = 0.3$ MPa^{-1} , indicated by IK, Ibanez and Kronenberg 1993) and for fluid-saturated Kimmeridge Bay shale ($\alpha = 0.27$ MPa^{-1} at high strain rates, indicated by SCBM, Swan et al. 1989).

range in strain rate tested.

Previous investigation of Wilcox shale deformed at high confining pressures without pore fluids (Ibanez and Kronenberg 1993) revealed a relationship between ultimate strength and strain rate given by an exponential glide law of the form:

$$(3) \quad \dot{\epsilon} = A(T) \exp\{\alpha(\sigma_1 - \sigma_3)\}$$

where $A(T)$ depends on temperature and α is a material parameter. Although our experiments were conducted at relatively low effective pressures, the results over the range of strain rates investigated can similarly be fit by eqn. (3). The results displayed as $(\sigma_1 - \sigma_3)$ vs. $\ln \dot{\epsilon}$ define a slope ($= 1/\alpha$, Fig. 4A) with a value of $\alpha = 0.29$ MPa^{-1} (determined by least-squares methods) that is surprisingly similar to that ($\alpha = 0.3$ MPa^{-1}) determined for Wilcox shale (Ibanez and Kronenberg 1993) without pore fluids present (Fig. 4B). Strengths of Wilcox shale at elevated pressures are much greater than the failure strengths measured in this study at low effective pressures and brittle mechanisms of deformation play a much larger role in the deformation experiments reported here; yet the relationship between strength and rate of deformation is very similar. The results presented in this study reflect the undrained mechanical response of Wilcox shale and comparison with the results of Ibanez and Kronenberg (1993) suggests that strengths of shales, both for drained and undrained conditions, exhibit similar intrinsic dependencies upon the rate of deformation. Swan et al. (1989) reported an intrinsic effect of strain rate on the undrained strength of fluid-saturated Kimmeridge Bay shale for strain rates of $1.7 \times 10^{-5} \leq \dot{\epsilon} \leq 1.7 \times 10^{-1} \text{ s}^{-1}$. Recasting their results as $(\sigma_1 - \sigma_3)$ vs. $\ln \dot{\epsilon}$ (Fig. 4B), the increases in strength they observed with increasing

strain rate (at $\dot{\epsilon} > 10^{-4} \text{ s}^{-1}$) yield a value of $\alpha = 0.27 \text{ MPa}^{-1}$, consistent with the results of this study and the relationship between strength and strain rate reported for high confining pressures (Ibanez and Kronenberg 1993).

The results of this study differ with those of Swan et al. (1989) at $\dot{\epsilon} \leq 10^{-4} \text{ s}^{-1}$. However, the conditions for fluid exchange between internal pores of specimens and reservoirs of the fluid pressure systems differ as well. The rate-dependent deformation of brine-saturated Wilcox shale is described by eqn. (3) over the entire range of strain rate ($2.8 \times 10^{-7} \leq \dot{\epsilon} \leq 8.2 \times 10^{-3} \text{ s}^{-1}$) investigated, whereas experiments performed on Kimmeridge Bay shale (Swan et al. 1989) show a transition in mechanical response at a strain rate of $\sim 10^{-4} \text{ s}^{-1}$ (Fig. 4B) with an inverse relationship between strength and strain rate at low strain rates attributed to partial drainage and relaxation of pore pressures.

The transition at which pore pressure drainage becomes significant and the magnitudes of pore pressures generated during deformation decay depend upon permeability and the scale at which fluid flow is important. Measurements of permeability at the same conditions as applied during deformation experiments indicate that characteristic times for pore pressure equilibration along the lengths of Wilcox shale specimens are long ($2 \times 10^5 \text{ s}$) and characteristic strain rates required to maintain near-equilibrium pore pressures during deformation (over strain increments of $\sim 0.1\%$) are low ($\dot{\epsilon} < 4 \times 10^{-9} \text{ s}^{-1}$). Pore pressure perturbations generated during deformation may remain large (with less than 10% relaxation) at the specimen scale at strain rates $\dot{\epsilon} > 6 \times 10^{-7} \text{ s}^{-1}$; the lack of significant fluid pressure relaxation predicted by our permeability results are consistent with the mechanical results for fluid-saturated Wilcox shale. The absolute strengths of shales may depend upon pore fluid flow at finer scales and the changes in pore fluid pressures measured during deformation indicate that some fraction of pores is better connected than implied by the macroscopic measures of permeability. Nevertheless, pores that are not drained are likely to contribute most to weakening specimens and the results for Wilcox shale at strain rates as low as $2.8 \times 10^{-7} \text{ s}^{-1}$ appear to reflect this.

The permeability of Kimmeridge Bay shale ($k = 8 \times 10^{-21} \text{ m}^2$ at an effective pressure of 10 MPa, Swan et al. 1989) is essentially the same as determined for Wilcox shale (at $P_c - P_f = 5.5 \text{ MPa}$). However, the experiments of Swan et al. (1989) allowed for radial exchange of pore fluids between specimens and fluid reservoirs of their apparatus. The shortened length scale for radial fluid transport shifts the transitional mechanical behavior between fully drained and undrained responses to higher strain rates and helps explain the differences in mechanical results reported for these two shales.

The results for Wilcox and Kimmeridge Bay shales combined indicate that the intrinsic mechanical properties of clay-bearing shales depend upon rates of deformation with similar stress-strain rate relationships for drained and undrained conditions. An inverse relationship between strength and strain rate, as reported by Swan et al. (1989), may be expected over an interval in strain rates; however, the conditions for this transitional behavior depend upon permeabilities and length scales of fluid flow that result in partial relaxation of pore pressure variations during deformation.

4 CONCLUSIONS

Based on the results of permeability measurements and deformation experiments on Wilcox shale, the following conclusions can be drawn:

1. The permeability of illite-rich shale depends upon effective pressure; measured values of k decrease with increasing effective pressure and are very low ($\sim 10^{-21} \text{ m}^2$) at $P_c - P_f \geq 5 \text{ MPa}$.

2. Permeability measurements for Wilcox shale indicate that equilibrium pore pressures cannot be maintained during deformation experiments at $\dot{\epsilon} > \sim 10^{-9} \text{ s}^{-1}$, consistent with the apparent undrained response of specimens at $\dot{\epsilon} > \sim 10^{-7} \text{ s}^{-1}$. Mechanical results over the range in strain rates investigated depart from a simple effective pressure law and appear to represent the response of illite-bearing shale without

significant relaxation of pore pressure perturbations generated during deformation.

3. Fracture strengths ($\sigma_1 - \sigma_3$) of Wilcox shale specimens saturated (as nearly as can be achieved) with pore fluids increase with increasing strain rates $\dot{\epsilon}$ over the range $2.8 \times 10^{-7} \leq \dot{\epsilon} \leq 8.2 \times 10^{-3} \text{ s}^{-1}$ and fit an exponential relationship $\dot{\epsilon} = A \exp(\alpha(\sigma_1 - \sigma_3))$ with a value of $\alpha = 0.29 \text{ MPa}^{-1}$ nearly identical to that measured at high confining pressures ($\alpha = 0.3 \text{ MPa}^{-1}$) without pore fluids.

5 ACKNOWLEDGMENTS

Special thanks go to Dr. J. Holder for many helpful discussions during the course of this study and for technical suggestions that made these measurements possible. We also thank Dr. R. Berg for discussions regarding the geologic roles of shales and for providing the shale core for study. This study was supported in part by the U.S. Department of Energy (Grant No. DE-FG05-87ER13711) and by a cooperative Industrial Associates Research Program with member companies including Conoco Inc., Shell Development Co., Union Pacific Resources, and Unocal Corporation; their contributions to this study are gratefully acknowledged.

REFERENCES

- Bauer, R.A. 1979. The loss of natural moisture content of Pennsylvanian shale and effect on physical properties. *Proc. Ill. Mining Inst., 87th Annual Meeting*: 13-28.
- Brace, W.F., J.B. Walsh & W.T. Frangos 1968. Permeability of granite under high pressure. *J. Geophys. Res.* 73: 2225-2236.
- Bishop, R.S. 1977. Shale diapir emplacement in South Texas - LaWard and Sherriff examples. *Gulf Coast Geol. Soc. Trans.* 27: 20-28.
- Chapple, W.M. 1978. Mechanics of thin-skinned fold-and-thrust belts. *Geol. Soc. Amer. Bull.* 89: 1189-1198.
- Cook, J.M. & M. Thiercelin 1989. Indentation resistance of shale: The effects of stress state and strain rate. In *Rock mechanics as a guide for efficient utilization of natural resources, Proc. 30th U.S. Symp. Rock Mech.*, ed A.W. Khair, 757-764.
- Ibanez, W.D. & A.K. Kronenberg 1993. Experimental deformation of shale: Mechanical properties and microstructural indicators of mechanisms. *Int. J. Rock Mech. Min. Sci. & Geomech. Abstr.* 30: 723-734.
- Mesri, G. & R. Gibala 1972. Engineering properties of a Pennsylvanian shale. In *Stability of rock slopes, Proc. 13th U.S. Symp. Rock Mech.*, 57-75.
- Meyer, C.A., R.B. McClintock, G.J. Silvestri & R.C. Spence, Jr. 1979. *ASME Steam table, Thermodynamic and transport properties of steam*, The American Society of Mechanical Engineers.
- Nuesch, R. 1991. *Das mechanische Verhalten von Opalinuston*. Ph.D. thesis, Eidgenossischen Technischen Hochschule, 244 pp.
- Rice, J.R. & M.P. Cleary 1976. Some basic stress diffusion solutions for fluid-saturated elastic porous media with compressible constituents. *Rev. Geophys. Space Phys.* 14: 227-241.
- Roeloffs, E.A. 1988. Fault stability changes induced beneath a reservoir with cyclic variations in water level. *J. Geophys. Res.* 93: 2107-124.
- Shea, W.T. & A.K. Kronenberg 1992. Rheology and deformation mechanisms of an isotropic mica schist. *J. Geophys. Res.* 97: 15201-15237.
- Steiger, R.P. & P.K. Leung 1990. Predictions of wellbore stability in shale formations at great depth. In *Rock at great depth*, eds. V. Maury & D. Foumaintraux, 1209-1218.
- Sutherland, H.J. & S.P. Cave 1980. Argon gas permeability of New Mexico rock salt under hydrostatic compression. *Int. J. Rock Mech. Min. Sci. & Geomech. Abstr.* 17: 281-288.
- Swan, G., J. Cook, S. Bruce & R. Meehan 1989. Strain rate effects in Kimmeridge Bay shale. *Int. J. Rock Mech. Min. Sci. & Geomech. Abstr.* 26: 135-149.
- Van Eeckhout, E.M. 1976. The mechanisms of strength reduction due to moisture in coal mine shales. *Int. J. Rock Mech. Min. Sci. & Geomech. Abstr.* 13: 61-67.